Indium oxide (In_2O_3) nanoparticles using *Aloe vera* plant extract: Synthesis and optical properties

S. MAENSIRI[a,b*], P. LAOKUL[a], J. KLINKAEWNARONG[a], S. PHOKHA[a], V.PROMARAK[c], S. SERAPHIN[d]
[a]*Small & Strong materials Group (SSMG), Department of Physics, Faculty of Science, Khon Kaen University, Khon Kaen, 40002, Thailand*
[b]*Integrated Nanotechnology Research Center (INRC), Khon Kaen University, Khon Kaen, 40002, Thailand*
[c]*Advanced Organic Materials and Devices Laboratory, Department of Chemistry, Faculty of Science, Ubon Ratchathani University, Varinchamrap, Ubon Ratchathani 34190, Thailand*
[d]*Department of Materials Science and Engineering, The University of Arizona, Tucson, Arizona 85721, USA*

In_2O_3 nanoparticles with particle sizes of 5-50 nm were synthesized by a simple, cost effective and environmental friendly route using indium acetylacetonate and *Aloe vera* plant extracted solution. The precursor was characterized by TG-DTA to determine the thermal decomposition and crystallization temperature which was found to be at above 350 °C. Nanoparticles are formed after calcination the dried precursor of In_2O_3 in air at 400-600°C for 2 h. Structural, morphological and optical properties of the synthesized nanoparticles were characterized. XRD and TEM analysis showed that the In_2O_3 samples are cubic with particle sizes of 5-50 nm. The morphology and size of In_2O_3 materials were affected by the calcination temperature. The prepared In_2O_3 nanoparticles showed a strong PL emission in the UV region. The strong emissions of In_2O_3 are attributed to the radioactive recombination of an electron occupying oxygen vacancies with a photo-excited hole. The present work proves that the *Aloe vera* plant-extracted solution synthesis is a new useful method using cheap precursors for preparation of In_2O_3 nanoparticles.

(Received February 1, 2008; accepted March 13, 2008)

Keywords: Indium oxide, Nanoparticles, Synthesis, Electron microscopy, Photoluminescence

1. Introduction

Indium oxide (In_2O_3) is an important n-type semiconductor with wide direct band-gaps of 3.55-3.75 eV. It has interesting properties such as high transparency to visible light, high electrical conductance, and strong interaction between certain poisonous gas molecules and its surfaces [1-3]. These properties make In_2O_3 an interesting material for a variety of applications, including solar cells [1,2], panel displays [4], organic light emitting diodes [5], photocatalysts [6], architectural glasses [7], field emission [8]. Moreover, In_2O_3 is an important material for semiconductor gas sensors [9-14]. Recently, investigations on preparation of In_2O_3 nanostructures with various forms such as nanotubes [15], nanobelts [16-18], nanofibers [19,20], wires [21-28], and nanoparticles [29-31] have been widely emphasized to extend their technological applications. Among these nanostructures, In_2O_3 with nanoparticulate form has been intensively studied to be used as a promising material for gas sensor applications. So far, nanoparticles of In_2O_3 have been synthesized by several techniques including sol–gel technique [9,12,32], pulse laser deposition [29], thermal decomposition [30,33,34], thermal hydrolysis [35], microemulsion [31,36], spray pyrolysis [37], mechanical chemical processing [38], hybrid induction and laser heating (HILH) method [39], nonaqueous synthesis [40], and hydrothermal synthesis [41]. Among other established synthesis methods, simple and cost effective routes to synthesize nanocrystalline In_2O_3 by utilization of cheap, nontoxic and environmentally benign precursors are still the key issues.

Aloe vera (*Aloe barbadensis Miller*) is a perennial succulent belonging to the Liliaceal family, and it is a cactus-like plant that grows in hot, dry climates [42]. For many years, aloe vera has been reported to possess immunomodulatory, anti-inflammatory, UV protective, antiprotozoal, and wound- and burn-healing promoting properties [43-46]. Recently, the extract of *Aloe vera* plant has been successfully used to synthesize single crystalline triangular gold nanoparticles (~50-350 nm in size) and spherical silver nanoparticles (~15 nm in size) in high yield by the reaction of aqueous metal source ions (chloroaurate ions for Au and silver ions for Ag) with the extract of the *Aloe vera* plant [47]. To the best of our knowledge, this biosynthetic route has not been extended to the preparation of oxide materials.

Here, we report for the first time the novel synthesis of In_2O_3 nanoparticles with particle sizes of 5-50 nm using indium acetylacetonate and *Aloe vera* plant extracted solution. Nanoparticles are formed after calcination the dried precursor of In_2O_3 in air at 400-600°C for 2 h. This method utilizes *Aloe vera* plant extracted solution as a solvent instead of organic solvents. The advantages of this method include (i) use of cheap, nontoxic and environmentally benign precursors and (ii) simple procedures without time-consuming polymerization and problem with treatment of a highly viscous polymeric

resin. The current simple synthetic method using cheap precursors of *Aloe vera* plant extract provides high-yield nanosized materials with well crystalline structure and good optical properties, and the method can be used to prepare nanocrystalline oxides of other interesting materials.

2. Experimental

In this study, indium (III) acetylacetonate (99.99+ % purity, Aldrich) was used as the starting chemical material for In_2O_3. *Aloe vera* extracted solution was prepared from a 35 g portion of thoroughly washed *Aloe vera* leaves which were finely cut and boiled in 100 ml of de-ionized water. The resulting extract was used as an *Aloe vera* extract solution. In the preparation of In_2O_3 nanoparticles, 3 g of indium (III) acetylacetonate was first dissolved in 30 ml *Aloe vera* extract solution under vigorous stir at 60°C for several hours until dried. The dried precursor was crushed into powder using mortar and pestle. The precursor was characterized by to thermogravimetric-differential thermal analysis (TG-DTA) (Pyris Diamond TG-DTA, Perkin Elmer Instrument) to determine the thermal decomposition and crystallization temperature which was found to be at above 350 °C (Fig. 1). The dried precursor was ground and subsequently calcined in box-furnace at 400, 500, and 600°C for 2 h in air. The dried precursors and calcined samples of In_2O_3 were characterized for crystal phase identification by powder X-ray Diffraction (XRD) using a Philips X-ray diffractometer (PW3040, The Netherlands) with CuK_α radiation (λ = 0.15406 nm). The particle size and morphology of the calcined powders were characterized by transmission electron microscopy (TEM, Hitachi H8100 200 kV). The optical absorption spectra were measured in the range of 200-800 nm using a UV-3101PC UV-VIS-NIR scanning spectrometer (Shimadzu, Japan). Photoluminescence (PL) measurement was carried out on a luminescence spectrometer (Perkin–Elmer LS-55B, PerkinElmer Instrument, USA) using a Xenon lamp as the excitation source at room temperature. The samples were dispersed in dichloromethane and the excitation wavelength used in PL measurement was 250 nm.

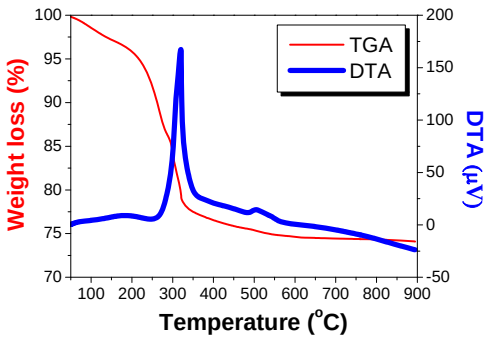

Fig. 1. TG-DTA curves of thermal decomposition of In_2O_3 precursor at a heating rate of 10 °C/min in static air.

3. Results and discussion

The thermogravimetric-differential thermal analysis (TG-DTA) curves of as-prepared In_2O_3 precursor are shown in Fig. 1. The TG curve in Fig. 1 shows a major weight loss step from 190°C up to about 350°C with slightly weight loss from 350°C to 600°C, and no further weight loss was observed at above 600°C. The weight loss is related to the combustion of organic matrix. On the DTA curve (Fig. 1) a main exothermic effect was observed between 260°C and 360°C with a maximum at about 320°C, indicating that the thermal events can be associated with the burnout of organic species involved in the precursor powders (organic mass remained from *Aloe vera* extract), of the residual carbon or due to direct crystallization of nanocrystalline In_2O_3 from the amorphous component. The formation of nanocrystalline In_2O_3 as decomposition product was confirmed by XRD and Raman results shown in Figure 2 and 3. The XRD patterns of In_2O_3 samples are show in Figure 2. All of the detectable peaks (Figure 2) can be indexed as the In_2O_3 cubic structure in the standard data (JCPDS: 06-0416). The cubic lattice parameter *a* calculated from the XRD spectra are 1.0118(5), 1.0105(2), and 1.0096(4) Å for In_2O_3 samples calcined at 400, 500, and 600°C, respectively. The crystallite sizes of the powders were estimated from X-ray line broadening using Scherrer's equation [48] (i.e. $D = 0.89\lambda/(\beta\cos\theta)$, where λ is the wavelength of the X-ray radiation, *K* is a constant taken as 0.89, θ is the diffraction angle, β is the full width at half maximum (*FWHM*)), and were obtained to be 13 ± 1, 15 ± 4, and 15 ± 3 nm for In_2O_3 samples calcined at 400, 500, and 600°C, respectively. The particle sizes and lattice parameters of In_2O_3 samples are also summarized in Table 1.

Table 1. Average particle sizes from XRD line broadening, cubic lattice parameter a calculated from XRD spectra and the band gap (E_g) of the nanocrystalline In_2O_3 samples calcined in air at different temperatures for 2 h.

In_2O_3 sample	Average particle size (nm)		Cubic lattice parameter *a* (Å)	Estimated band gap (eV)
	from XRD	From TEM		
Calcined at 400°C	13 ± 1	5-10	1.0118(5)	3.25
Calcined at 500°C	15 ± 4	10-25	1.0105(2)	3.31
Calcined at 600°C	15 ± 3	30-50	1.0096(4)	3.29

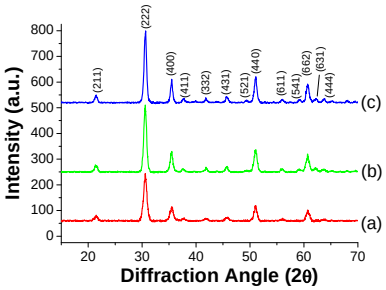

Fig. 2. XRD patterns of nanocrystalline In_2O_3 samples calcined in air for 2 h at (a) 400 °C, (b) 500 °C, and (c) 600°C.

The morphology and structure of the In_2O_3 samples were investigated by TEM. It is clear from the TEM bright-field images (Figure 3) that the morphology and size of In_2O_3 materials is affected by the calcination temperature. The TEM bright-field images of In_2O_3 (Fig. 3) show that the In_2O_3 sample calcined at 400 °C contains nanoparticles having sizes of ~5-10 nm whereas the In_2O_3 sample calcined at 500°C consists of well-dispersed particles of ~ 10-25 nm in diameter. The In_2O_3 sample calcined at 600 °C consists of larger particles with particle sizes in the ranges of 30-50 nm. The corresponding selected-area electron diffraction (SAED) patterns (Fig. 3) of all the In_2O_3 samples show spotty ring patterns without any additional diffraction spots and rings of second phases, revealing their crystalline cubic structure. Increase in calcination temperature results in stronger spotty pattern and the In_2O_3 samples calcined at 500, and 600 °C shows strong spotty patterns, indicating large particle size of highly crystalline cubic structure. Measured interplanar spacings (d_{hkl}) from selected-area electron diffraction patterns in Fig. 3 are in good agreement with the values in the standard data (JCPDS: 06-0416) as summarized in Table 2.

Table 2. Interplanar spacings (d_{hkl}) of In_2O_3 samples calculated from TEM selected-area electron diffraction patterns in Figure 3 compared with the reference values in the standard data (JCPDS: 06-0416).

Ring	Calculated interplanar spacing (d_{hkl}) In_2O_3 sample (Å)			Standard data (JCPDS: 06-0416)	
	In_2O_3 sample calcined at 400°C	In_2O_3 sample calcined at 500°C	In_2O_3 sample calcined at 600°C	d_{hkl} (Å)	h k l
R_1	3.08128	3.04418	3.13216	3.1234	111
R_2	2.72131	2.64079	2.75391	2.7056	200
R_3	1.91022	1.88178	1.93031	1.9134	220
R_4	1.67377	1.63154	1.65155	1.6318	311
R_5	1.57475	1.54755	1.57095	1.5622	222
R_6	1.36999	1.31635	1.36613	1.353	400
R_7	1.24260	1.23754	1.26204	1.2414	331
R_8	-	-	1.20599	1.2101	420
R_9	1.12631	1.10751	1.11244	1.1047	422
R_{10}	1.05124	1.04038	1.04829	1.0414	511
R_{11}	0.97570	0.96132	0.96307	0.9566	440
R_{12}	0.91377	0.90689	0.92393	0.9147	531

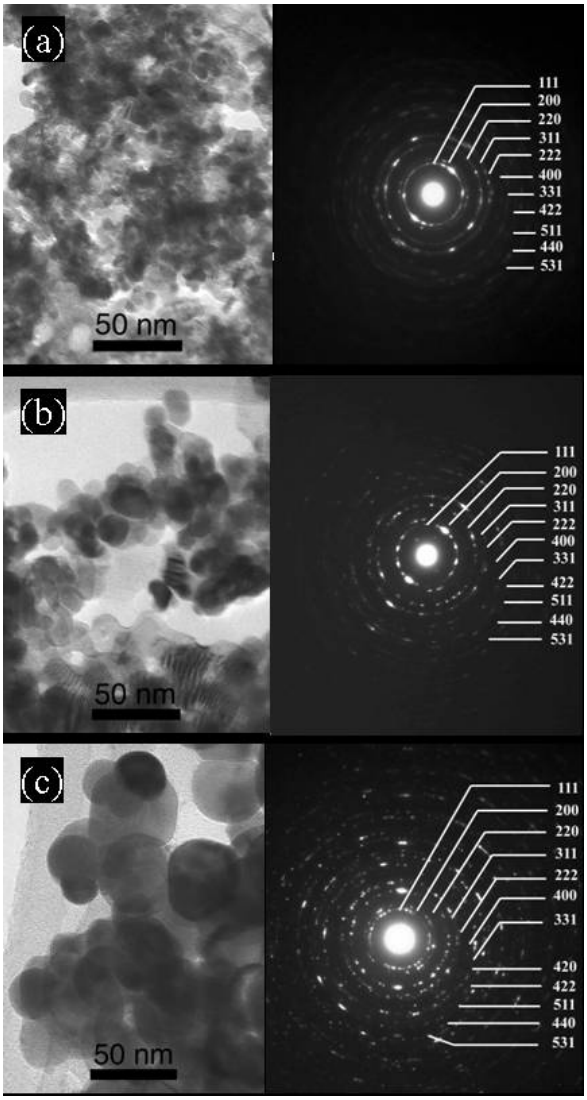

Fig. 3. TEM images with corresponding selected area electron diffraction (SAED) patterns of the nanocrystalline In_2O_3 samples calcined in air for 2 h at (a) 400°C, (b) 500°C, and (c) 600°C.

Now let us consider the optical properties of the In_2O_3 samples. The UV-visible absorption spectra of all the In_2O_3 samples (Figure 4) exhibit a strong absorption below 450 nm (2.76 eV) with a well defined absorbance peak at around 288 nm (4.31 eV). The direct band gap energy (E_g) of the samples is determined by fitting the absorption data to the direct transition equation: $\alpha h\nu = E_D\left(h\nu - E_g\right)^{1/2}$, where α is the optical absorption coefficient, $h\nu$ is the photon energy, E_g is the direct band gap, and E_D is a constant [49]. Plotting $(\alpha h\nu)^2$ as a function of photon energy, and extrapolating the linear portion of the curve to the absorption equal to zero as shown in the insets of Figure 4 gives the values of the direct band gap (E_g) to be 3.29 eV, 3.31 eV, and 3.25 eV for the In_2O_3 samples calcined at 400, 500, and 600°C, respectively. This value is lower than that of ~3.6 eV for the In_2O_3 reported in the literature [50].

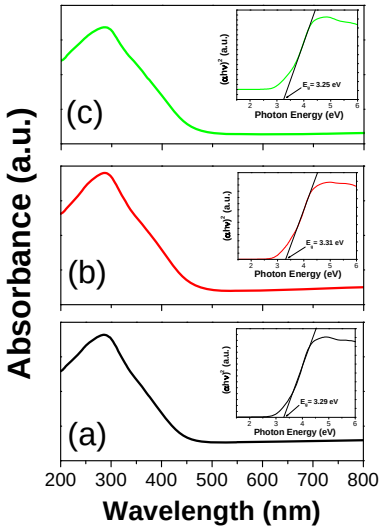

Fig. 4. Room temperature optical absorbance spectra of nanocrystalline In_2O_3 samples calcined in air for 2 h at (a) 400 °C, (b) 500 °C, and (c) 600 °C. The insets show plots of $(\alpha h\nu)^2$ as a function of photon energy, E.

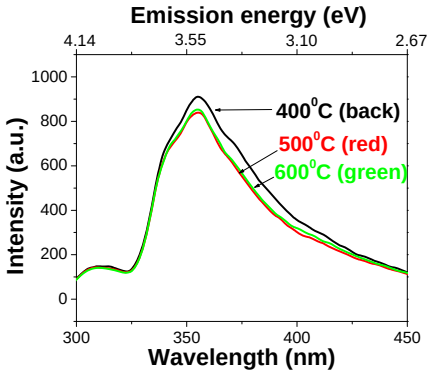

Fig. 5. Room temperature photoluminescence spectra of the synthesized nanocrystalline In_2O_3 samples calcined in air for 2 h at 400, 500, and 600 °C. The samples were dispersed in dichloromethane and the excitation wavelength used in PL measurement 250 nm.

Fig. 5 shows the room temperature PL spectra of the nanocrystalline In_2O_3 samples measured using a Xenon laser of 250 nm as an excitation source. The spectra of all the samples mainly consist of a strong UV emission broad band having emission maximum at ~ 354 nm (3.51 eV). The spectra of all the samples also show a weak UV band at ~308 nm (4.03 eV) and at ~ 371 nm (3.31 eV). It is well known that the bulk In_2O_3 cannot emit light at room temperature [51]. However, PL emissions of our nanocrystalline In_2O_3 samples are possibly due to the effect of the oxygen vacancies as reported in literatures [14,17,19,20,29,30,52-54]. In the present work, oxygen vacancies would be generated due to the partial or incomplete oxidation of precursor during the calcination. Moreover, small In_2O_3 particles would favor the existence of oxygen vacancies as found in In_2O_3 nanowires with high aspect ratios and high surface-to-volume ratio [17,19,54]. The oxygen vacancies would generally act as deep defect donors and cause the formation of new energy levels in the band gap of In_2O_3 samples. Thus, the PL emission from In_2O_3 nanoparticles results from the radioactive recombination of an electron occupying oxygen vacancies with a photo-excited hole, which is analogous to the photoluminescence mechanism of ZnO and SnO_2 semiconductors [19,52,54]. It should be noted that the weaker UV emission observed on the samples calcined at 500 and 600°C compared to that of the sample calcined at 400°C may be due to their lower sensitizing centers. It is clearly seen from TEM results (Figure 3) that as the calcination temperature increases, the crystal size of In_2O_3 samples becomes larger. As a result, the number of sensitizing centers decreases owing to reductions in both the ratio surface area and concentration of oxygen vacancies, thus results in a decrease in PL intensity as observed in ZnO nanoparticles reported by Du et al. [55].

4. Conclusions

We have synthesized nanoparticles of In_2O_3 by a simple method using *Aloe vera* plant extract solution. Structural, morphological and optical properties of the synthesized nanoparticles were characterized. XRD and TEM analysis showed that the In_2O_3 samples are cubic with particle sizes of 5-50 nm. The morphology and size of In_2O_3 materials were affected by the calcination temperature. The prepared In_2O_3 nanoparticles showed a strong PL emission in the UV region. The strong emissions of In_2O_3 are attributed to the radioactive recombination of an electron occupying oxygen vacancies with a photo-excited hole. The present work proves that the *Aloe vera* plant-extracted solution synthesis is a new useful method using cheap precursors for preparation of In_2O_3 nanoparticles. The current simple, cost effective and environmental friendly synthesis method using *Aloe vera* plant-extracted solution gives a potential avenue for further practical scale-up of the production process and applications. Moreover, it can be extended to prepare nanoparticles of other interesting oxide materials. However, the role of the aloe vera extract is not yet specified. For example, complexation between aloe vera components and zinc in the solution is still unknown, and this is under investigation.

Acknowledgments

The authors would like to thank the Department of Chemistry, Khon Kaen University for providing TG-DTA, UV-VIS-NIR spectroscopy facilities. This work is supported by The Integrated Nanotechnology Research Center (INRC), Khon Kaen University.

References

[1] I. Hamburg, C. G. Granqvist, J. Appl. Phys. **60**, R123 (1986).
[2] C. G. Granqvist Appl. Phys. A: Solid Surf. **57**, 19 (1993).

[3] K.G. Gopchandran, B. Joseph, J.T. Abraham, P. Koshy, V.K. Vaidyan, Vacuum, **86**, 547 (1997).
[4] Y. Zhang, H. Ago, J. Liu, M. Yumura, K. Uchida, S. Ohshima, S. Iijima, J. Zhu, X. Zhang, J. Cryst. Growth. **264**, 363 (2004).
[5] J. Lao, J. Huang, D. Wang, Zhifeng Ren, Adv. Mater. 16, **65** (2004).
[6] H. Zhu, N. Wang, L. Wang, K. Yao, X. Shen, Inorg. Mater. **41**, 609 (2005).
[7] X. Chen, Z. Zhang, X. Zhang, J. Liu, Y. Qian, Chem. Phys. Lett. **407**, 482 (2005).
[8] S. Kar, S. Chakrabarti, S. Chaudhuri, Nanotechnology. **17**, 3058 (2006).
[9] A. Gurlo, M. Ivanovskaya, N. Barsan, M. Shweizer-Berberich, U. Weimar, W. Gopel, A. Dieguez, Sens. Actuat. B. **44**, 327 (1997).
[10] E. Comini, A. Cristalli, G. Faglia, Gg. Sberveglieri, Sens. Actuat. B. **65**, 260 (2000).
[11] H. Steffes, C. Imawan, F. Solzbacher, F. Solzbacher, Obermeier, Sens. Actuat. B. **68**, 249 (2000).
[12] M. Ivanovskaya, A. Gurlo, P. Bogdanov, Sens. Actuat. B. **77**, 264 (2001).
[13] A. Gurlo, N. Barson, U. Weimar, M. Ivanovskaya, A. Tuarino, P. Siciliano, Chem. Mater. **15**, 4377 (2003).
[14] Q. Tang, W. Zhou, W. Zhang, S. Ou, K. Jiang, W. Yu, Y. Qian, Cryst. Growth Des. **5**, 147 (2005).
[15] X.-P. Shen, H.-J. Liu, Z. Fan, Y. Jiang, J.-M. Hong, Z. Xu, J. Cryst. Growth. **276**, 471 (2005).
[16] H. J. Chen, Y. S. Choi, S. Y. Bae, J. Park, Appl. Phys. A. **81**, 539 (2005).
[17] J. S. Jeong, J. Y. Lee, C. J. Lee, S. J. An, G.-C. Yi, Chem. Phys. Lett. **384**, 246 (2004).
[18] T. Gao, T. Wang, J. Cryst. Growth. **290**, 660 (2006).
[19] C. H. Liang, G. W. Meng, Y. Lei, F. Phillipp, L. D. Zhang, Adv. Mater. **13**, 1330 (2001).
[20] Y. Zhang, J. Li, Q. Li, L. Zhu, X. Liu, X. Zhong, J. Meng, X. Cao, Scripta Mater. **56**, 409 (2007).
[21] X. S. Peng, Y. W. Wang, J. Zhang, X. F. Wang, L. X. Zhao, G. W. Meng, L. D. Zhang, Appl. Phys. A. **74**, 437 (2002).
[22] X. C. Wu, J. M. Hong, Z. J. Han, Y. R. Tao, Chem. Phys. Lett. **373**, 28 (2003).
[23] J. Lao, J. Huang, D. Wang, Z. Ren, Adv. Mater. **16**, 65 (2004).
[24] K. Kam, F. L. Deepak, A. K. Cheetham, C. N. R. Rao, Chem. Phys. Lett. **297**, 329 (2004).
[25] Y. Zhang, H. Ago, J. Liu, M. Yumura, K. Uchida, S. Ohshima, S. Iijima, J. Zhu, X. Zhang, J. Cryst. Growth. **264**, 363 (2004).
[26] S. Q. Li, Y. X. Liang, T. H. Wang, Appl. Phys. Lett. **88**, 053107 (2006).
[27] S. Kar, S. Chakrabarti, S. Chaudhuri, Nanotechnology. **17**, 3058 (2006).
[28] G. Cheng, E. Stren, S. Guthrie, M. A. Reed, R. Klin, Y. Hao, G. Meng, L. Zhang, Appl. Phys. A. **85**, 233 (2006).
[29] A. Murali, A. Barve, V. L. Leppert, S. H. Risbud, Nano Lett. **1**, 287 (2001).
[30] W. S. Seo, H. H. Jo, K. Lee, J. T. Park, Adv. Mater. **15**, 795 (2003).
[31] Z. Zhan, W. Song, D. Jiang, J. Colloid Interf. Sci. **271**, 366 (2004).
[32] M. Epifani, P. Siciliano, J. Am. Chem. Soc. **126**, 4078 (2004).
[33] H. Zhou, W. Cai, L. Zhang, Mater. Res. Bull. **34**, 845 (1999).
[34] J. F. Q. Rey, T. S. Plivelic, R. A. Rocha, S. K. Tadokoro, I. Torriana, E. N. S. Muccillo, J. Nanopart. Res. **7**, 203 (2005).
[35] B. Yu, Acta Phys. Sinica. **48**, 320 (1999).
[36] X. J. Wu, J. Vac. Sci. Technol. **15**, 1889 (1997).
[37] J. J. Prince, S. Ramamurthy, B. Subramanian, J. Cryst. Growth. **240**, 142 (2002).
[38] H. Yang, A. Tang, X. Zhang, W. Yang, G. Qiu, Scripta Mater. **50**, 413 (2004).
[39] B. L. Zhu, C. S. Xie, D. W. Zeng, A. H. Wang, W. L. Song, X. Z. Zhao, J. Mater. Sci. Lett. (2005) 0022.
[40] M. Niederberger, G. Garnweitner, J. Buha, J. Polleux, J. Ba, N. Pinna, J. Sol-Gel. Sci. Tech. **40**, 259 (2006).
[41] J. Xu, X. Wang, J. Shen, Sens. Actuat. B. **115**, 642 (2006).
[42] S. Choi, M.-H. Chung, Seminar. Integrat. Med. **1**, 53 (2003).
[43] T. Reynolds, A. C. Dweck, J. Ethnopharmacol. **68**, 3 (1999).
[44] K. H. Shin, W. S. Woo, S. S. Lim, C. S. Shim, H. S. Chung, E. J. Kennely, A. D. Kinghorn, J. Nat. Prod. **60**, 1180 (1997).
[45] K. Umano, K. Nakahara, A. Shoji, T. Shibamoto, J. Agric. Food Chem. **47**, 3702 (1999).
[46] D. Saccu, P. Bagoni, G. J. Procida, J. Agric. Food Chem. **49**, 4526 (2001).
[47] S. Prathap Chandran, M. Chaudhary, R. Pasricha, A. Ahmad, M. Sastry, Biotechnol. Prog. **22**, 577 (2006).
[48] B. D. Cullity, S. R. Stock, "Elements of X-ray Diffraction", Printice Hall, New Jersey, 3nd ed. (2001).
[49] E. Ziegler, A. Heinrich, H. Oppermann, G. Stover, Phys. Status Solidi A, **66**, 635 (1981).
[50] C. G. Granqvist, Appl. Phys. A **57**, 19 (1993).
[51] Y. Ohhata, F. Shinoki, S. Yoshida, Thin Solid Films **59**, 255 (1979).
[52] M. S. Lee, W. C. Choi, E. K. Kim, C. K. Kim, S. K. Min, Thin Solid Films **279**, 1 (1996).
[53] H. J. Zhou, W. P. Cai, L. D. Zhang, Appl. Phys. Lett. **75**, 495 (1999).
[54] J. Zhang, X. Qing, F. Jiang, Z. Dai, Chem. Phys. Lett. **371**, 311 (2003).
[55] Y. Du, M.-S. Zhang, J. Hong, Y. Sheen, Q. Chen, Z. Yin, Appl. Phys. A. **76**, 171 (2003).

*Corresponding author: sanmae@kku.ac.th;
santimaensiri@gmail.com